ACS APPLIED MATERIALS & INTERFACES

Research Article

www.acsami.org

Amine-Capped Co Nanoparticles for Highly Efficient Dehydrogenation of Ammonia Borane

Jiantong Hu, Zhongxin Chen, Mengxiong Li, Xiaohui Zhou, and Hongbin Lu*

State Key Laboratory of Molecular Engineering of Polymers and Department of Macromolecular Science, Fudan University, Shanghai, 200433, P. R. China

Supporting Information

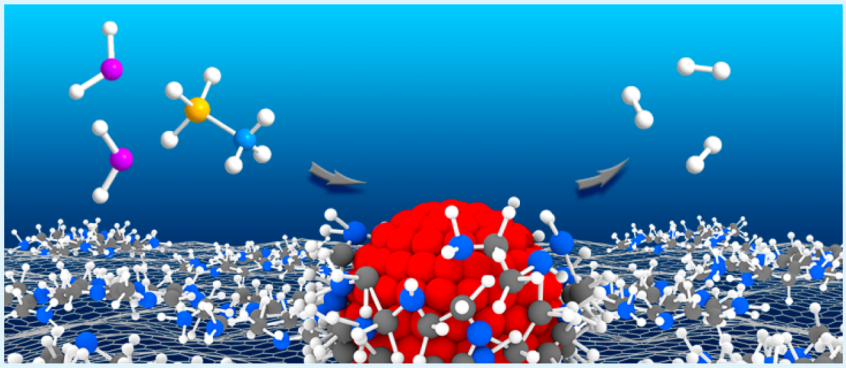

ABSTRACT: Highly efficient heterogeneous catalysts are desired for the development of new energy storage materials. The rational choice and use of capping ligands are of significant importance for performance optimization of metal nanoparticle (NP) catalysts. By exploiting amine-rich polyethylenimine (PEI) and graphene oxide (GO) as a NP support, we demonstrate that as a capping ligand, PEI deposited on GO provides a novel pathway able to simultaneously control the morphology, spatial distribution, surface active sites of cobalt (Co) NPs, and remarkably enhances their catalytic properties for the hydrolytic dehydrogenation of ammonia borane (AB). Such a synergistic effect enables the synthesized PEI-GO/Co catalysts to reveal extremely high dehydrogenation activities under atmosphere condition. A total turnover frequency of 39.9 mol_{H2} min^{-1} mol_{Co}^{-1} and an apparent activation energy of 28.2 kJ mol^{-1} make the catalytic performance of these PEI-GO/Co catalysts comparable to those of noble metal-based catalysts, including bimetallic and multimetallic catalysts.

KEYWORDS: *ammonia borane hydrolysis, heterogeneous catalysis, amine-capped, Co nanoparticles, graphene*

1. INTRODUCTION

The ever-growing concerns on energy crisis have stimulated intensive interest for the renewable energy and storage materials.[1] Hydrogen, a promising energy carrier with advantages of lightweight, highly abundant, clean, and high chemical energy per mass, has attracted considerable attention for satisfying the increasing energy demand.[2] To achieve practical applications, for example in hydrogen fuel cell field, seeking suitable hydrogen storage materials with high gravimetric/volumetric capacity of hydrogen and utilizing them at low temperature and pressure are two critical issues.[3] Owing to its high gravimetric hydrogen capacity of 19.6 wt %, stability, water solubility, and nontoxicity, ammonia borane (NH_3BH_3, AB) is deemed to be one of the most promising chemical hydrogen storage materials for future hydrogen economy.[4] There are two primary ways to release hydrogen from AB, that is, catalytic thermolysis and catalytic hydrolysis. The former allows for the regeneration of AB when hydrogen is not fully released, but it usually requires high temperature and hydrogen is commonly released at a relatively low rate.[5,6] In contrast, the hydrolysis of AB can proceed rapidly and generate three equivalents of H_2 at room temperature, provided that proper heterogeneous catalysts are employed.[7,8] This intriguing character has driven numerous efforts to develop novel catalysts for enhanced hydrolysis efficiency of AB.[9]

Given their element abundance and recycling capability, inexpensive transition metal catalysts such as Fe,[10] Co,[11] and Ni[12] have attracted considerable attention, revealing potential in prompting the hydrolytic dehydrogenation of AB. Nevertheless, further improving their catalytic efficiency remains a challenge. To this end, various kinds of support materials have been utilized to control the morphology of deposited nanoparticles (NPs) and maximize their reactive surface sites.[8,11,13−15] In spite of these significant improvements, their dehydrogenation efficiency is still low relative to those noble metal catalysts.[16,17] As demonstrated by Özkar et al., the majority of supported non-noble metal catalysts had a TOF value of <35 $mol_{H2}/min/mol_{metal}$, while plenty of noble metal

Received: May 19, 2014
Accepted: July 18, 2014
Published: July 18, 2014

catalysts showed a TOF value of >100 $mol_{H2}/min/mol_{metal}$.[18] Besides, noble metal catalysts often exhibited desired recycle stability. Nevertheless, the expensive cost for noble metal catalysts is a key issue that hinders their large-scale energy applications. This is the primary drive force to further develop for high performance earth abundant metal catalysts.

Nowadays, a new understanding on the role of capping ligands is opening a promising door for further developing highly active metal nanocatalysts.[19,20] The organic ligands coordinated to metal surfaces can tailor the metal−organic interfaces and enable the fabrication of excellent heterogeneous catalysts. Standing out from most cases, several specific ligand-capped NPs reveal superior advantages, which not only allow for stabilization of sized-controlled NPs, but also further promote the catalytic activities through synergistic effect. While such synergistic effects have been well recognized in bimetallic or multimetallic catalysts,[21−25] they are less realized in ligand-capped metal NPs. Only a few strategies have been documented to be effective for the capping ligand-prompted synergistic effect.[26−31] For instance, Tsunoyama et al. reported that poly(vinylpyrrolidone) (PVP), besides being a stabilizer, could increase the electron density of ultrasmall sized Au clusters, leading to an improved catalytic activity for aerobic oxidation of alcohol.[30] In addition, the amino and hydroxyl groups in 5,10,15,20-tetrakis(4-hydroxyphenyl) porphyrins (THPP) were also found to exhibit a similar contribution to the Pd clusters, where the π-conjugated system in THPP facilitated the charge transfer between catalyst and functional groups, and the coordination interaction prevented occurrence of the NPs aggregation in the electrocatalytic process.[31] As suggested by Li et al., the promoting role of capping ligands could be classified into five categories: charge transfer, surface crowding effect, molecular recognition, chiral modification, and adsorption regulation.[19] This implies that the existence of capping ligands may significantly affect the access pathway and adsorption energy of reactive substrates on NP surfaces via noncovalent interactions. However, how to take full advantages of the synergistic effect of capping ligands has been less explored, especially for the hydrolytic dehydrogenation of AB.

In this work, we demonstrate the strong synergistic effect of polyethylenimine (PEI)-capped Co NPs (PEI-GO/Co), which are deposited on GO, for the hydrolytic dehydrogenation of AB. The catalysts reveal a total turnover frequency of 39.9 $mol_{H2}\ min^{-1}\ mol_{Co}^{-1}$ and an activation energy of 28.2 kJ mol^{-1}, which are comparable with those of noble metal-based catalysts, for example, 40 wt % Pt/C.[32] The ultrahigh catalytic activity primarily stems from amine-promoted AB diffusion, dihydrogen bonds (DHBs) induced formation of activated species, as well as effective control in the morphology of Co NPs. These experimental results demonstrate the validity of amine-rich polymer capping ligands on constructing high performance heterogeneous nanocatalysts for the hydrolytic dehydrogenation of AB.

2. EXPERIMENTAL SECTION

2.1. Materials. Graphite powder 8099200 (120 μm) was purchased from Qingdao BCSM Co. 98% H_2SO_4, 65% HNO_3, 30% H_2O_2, 96.0% sodium borohydride, 99.0% 1,2-ethylenediamine (EDA), 99.0% triethylamine (TEA), poly(vinylpyrrolidone) (PVP, K-30, M_w = 40,000) were purchased from Sinopharm Chemical Regent Co., 99.5% diisopropylamine (DIPA) from Aladdin, sodium nitrate from Shanghai Qiangshun Chemical Co., $KMnO_4$ from Shanghai Zhenxin Chemical Co., polyethylenimine (PEI, M_w = 600, branched, and PEI, M_w = 25000, linear) and cobalt(II) acetate tetrahydrate from Alfa Aesar, poly(acrylic acid) (PAA, M_w = 2000, 63 wt % solution) from Acros, ammonia-borane complex (90%) from Aldrich. All chemicals were used as received. Deionized water (DI water) was used in all experiments.

2.2. Synthesis of PEI-GO/Co Catalysts. Graphene oxide (GO) was prepared by the Hummers method and freeze-dried before use. Ten milliliters of PEI (branched, M_w = 600) solution (100 mg mL^{-1}) was gradually added into 10 mL of GO solution (5 mg mL^{-1}). The pH value was adjusted at ∼11. The mixture solution was stirred magnetically at 60 °C for 24 h. After that, the mixture was purified by centrifugation and then freeze-dried to constant weight. PEI-GO/Co catalysts were prepared by in situ deposition of metal NPs on the PEI-GO surface. Typically, 10 mg of as-prepared PEI-GO was added to 20 mL of DI water in a two-necked round-bottom flask, with a constant pH ≈ 10. After stirring for 15 min, 0.2 mmol $Co(Ac)_2{\cdot}4H_2O$ was added to the above solution and stirred for another 30 min under nitrogen atmosphere. The color of the mixture changed into black immediately upon adding 20.0 mg of $NaBH_4$ by violent shaking. The reaction was kept until no visible hydrogen was released. The collected product was washed with DI water and ethanol and dried in a two-necked flask under the protection of nitrogen atmosphere.

2.3. Catalytic Hydrolysis of Ammonia-Borane (AB). The as-prepared PEI-GO/Co was dispersed into 18 mL of aqueous solution in a two-necked round-bottom flask. After that, 1.8 mmol AB dissolved in 2 mL DI water was injected into the catalyst solution with a syringe under vigorous stirring (1200 rpm). The reaction was carried out under ambient condition. The evolution of gas was monitored using a gas buret. In order to investigate the reactive kinetics, different concentrations of catalysts (2.5, 5, 7.5, 10 mM, corresponding PEI-GO's weights were 2.5, 5, 7.5, 10 mg, respectively) were used for dehydrogenation of 90 mM AB, and different molar ratios of ammonia borane (22.5, 45, 67.5, 90 mM) were also examined at 25 °C under ambient pressure, with a constant catalyst concentration (10 mM PEI-GO/Co). In addition, the effect of reaction temperature was studied at seven different temperatures (10, 15, 20, 25, 30, 35, 40 °C) for the dehydrogenation of 90 mM NH_3BH_3 catalyzed by 10 mM PEI-GO/Co. All the dehydrogenation experiments were monitored in the same way.

2.4. Recycle Stability Test of PEI-GO/Co Catalysts. After the dehydrogenation reaction was exhaustively completed, the catalyst was collected to the bottom of the flask with a magnet, and then the supernatant was removed carefully. Subsequently, 18 mL of DI water was added to the flask, and the new NH_3BH_3 dissolved in 2 mL of DI water was injected into the solution for testing the catalytic activity of the collected catalyst. The same process was repeated 5 times.

2.5. Characterization. Transmission electron microscopy (TEM, JEM-2100F and Tecnai G^2 20 Twin, both operating at 200 kV) was used to observe the morphology of PEI-GO/Co at different magnifications. All samples for imaging were prepared by depositing aqueous dispersions (∼0.2 mg mL^{-1}) on holey copper grids. Details of XPS, XRD, UV−vis, and other characterizations are presented in the Supporting Information.

3. RESULTS AND DISCUSSION

3.1. Synthesis and Characterization of PEI-GO/Co Catalysts. PEI-GO composites were prepared by a modified method based on our previous work.[33] It is worth noting that in condition close to neutral, amine groups readily react with carboxyl groups on GO by amidation reaction, which enables some of the amine groups of PEI to be converted into amide groups and reduces the number of amine groups.[34−36] To avoid this conversion, the reaction solution in the current study was adjusted to be alkaline (pH ∼11) so that the extent of amidation could be suppressed and most of the amine groups could be reserved, as revealed in the FT-IR and XPS spectra (Supporting Information Figure S3). TGA curves indicate that the amount of PEI attached on GO is ∼62 wt %, relative to GO. Further discussion on the structure and property of PEI-

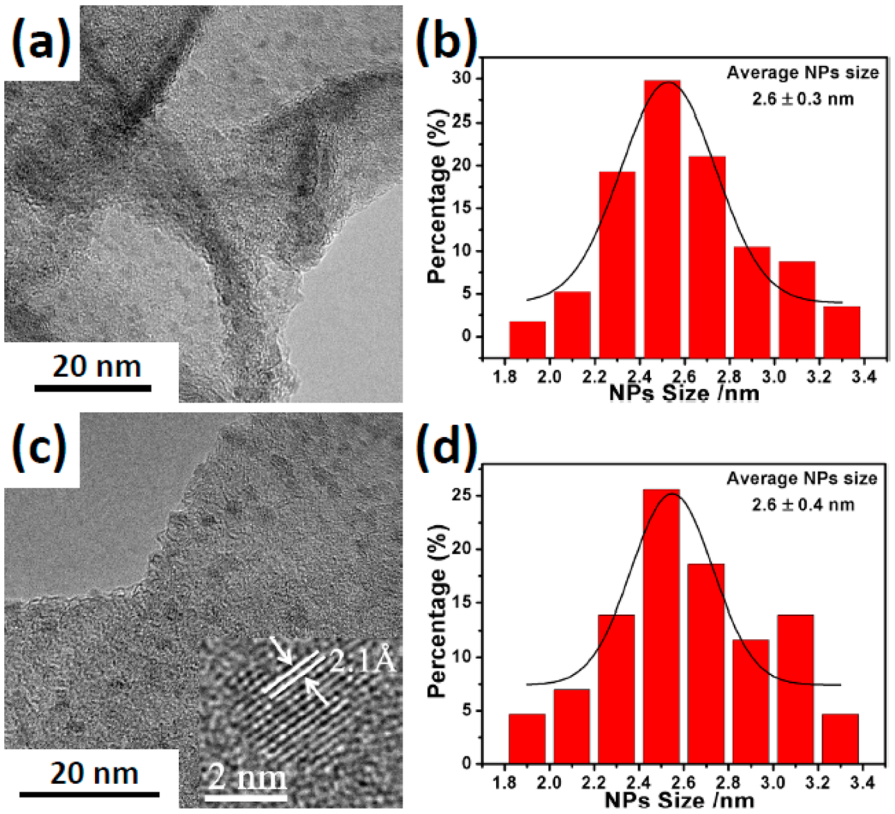

Figure 1. HR-TEM images and corresponding size histograms of (a, b) PEI/Co NPs and (c, d) PEI-GO/Co NPs. The average size is calculated from at least 100 NPs. Inset of panel c: The lattice spacing of crystallized Co NP, 0.21 nm.

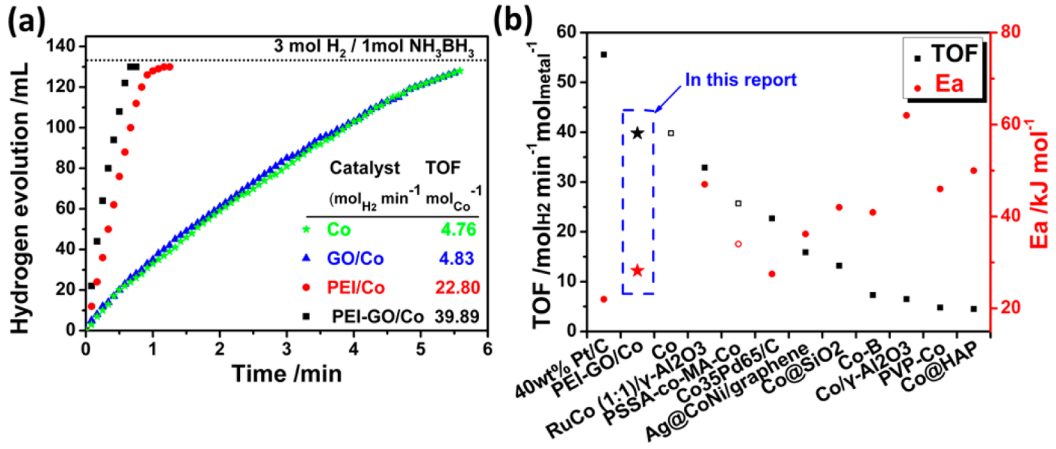

Figure 2. (a) Hydrogen generation rates of the AB hydrolysis in the presence of Co, GO/Co, PEI/Co, and PEI-GO/Co catalysts. (b) A comparison of our PEI-GO/Co catalyst with the reported Pt−C,[32] $Ru@Al_2O_3$,[38] Co-based monometallic,[8,10,39−43] bimetallic,[44,45] and trimetallic[46] catalysts in terms of TOF and E_a value using NH_3BH_3 or (NH_3BH_3 and $NaBH_4$) as the hydrogen source at room temperature (open plots, NH_3BH_3 and $NaBH_4$; solid plots, NH_3BH_3).

GO is presented in Supporting Information. According to Kobayashi et al.,[37] PEI consists of a repeating unit with one amine group and a $-CH_2-CH_2-$ spacer, implying that PEI on GO may provide numerous anchored coordination sites for Co^{2+} ions, see the schematic structure in Supporting Information Figure S2. The occurrence of coordination between amine and Co^{2+} ions reveals a color conversion, from light pink ($Co(Ac)_2$ solution) to orange ($Co(Ac)_2$/PEI solution). The UV−visible spectrum of cobalt acetate has a d-d absorption band at 520 nm. When Co^{2+} ions are chelated by amine groups of PEI, a new characteristic peak at a lower wavelength (224 nm) appears, belonging to the formation of PEI-Co^{2+} complex. The strong interaction between PEI and Co^{2+} suppressed the motion of reduced Co atoms when PEI-Co^{2+} was exposed to $NaBH_4$, so that Co NPs were able to be restricted within the PEI layer, and part of the coordinated amine ligands were preserved on the surface of NPs. At this point, PEI molecules played a critical role in controlling the size and morphology of Co NPs through steric effect and coordination interaction.

We employ HR-TEM to observe the morphology and spatial distribution of Co NPs on PEI and PEI-GO. These Co NPs

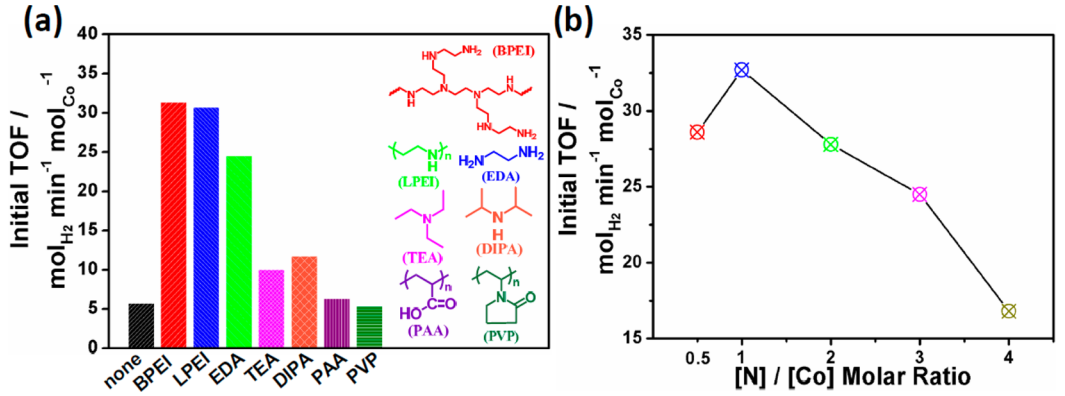

Figure 3. (a) Initial TOF values of AB hydrolysis catalyzed by Co NPs without or with different polymeric and amine capping agents; (b) the initial TOF values of PEI/Co catalysts at different molar ratio of [N]/[Co]. (Conditions: For amine molecules, PVP and PAA, the value of [N]/[Co], [C(O)N]/[Co], and [COOH]/[Co] were fixed at 1. [Co]: 10 mM. [AB]: 90 mM. Temperature: 25 ± 0.5 °C.)

formed are amorphous, as indicated by the XRD pattern in Supporting Information Figure S4. To discern the Co NPs, we allowed the sample to be exposed under electron beam for 1 min to facilitate the crystallization of Co NPs (Supporting Information Figure S8). From Figure 1, it is clear that the Co NPs are uniform in spatial distribution, and no obvious difference in the average diameter (~2.6 nm) is observed for PEI/Co and PEI-GO/Co samples. The inset of Figure 1c shows that the interplane spacing of the particle lattice is 0.21 nm, in accord with the {111} lattice spacing of face centered cubic (fcc) Co. Note that Co NPs could form aggregates in bulk solution or on bare GO surfaces (Supporting Information Figure S6), this reflects the critical role of PEI amine groups in stabilizing and controlling the growth of NPs through the steric effect and coordination interaction. The as-synthesized Co NPs are amorphous, implying that there are a large amount of Co atoms accessible on the surface. We anticipate that such specific structures of Co NPs could contribute to their catalytic performance, especially considering the affinity of PEI to AB, see below.

3.2. Catalytic Activity of PEI-GO/Co. We demonstrate the catalytic behavior of these Co NPs deposited on PEI-GO by the hydrolytic dehydrogenation of AB. To illustrate the role of PEI-GO as the support in improving the catalytic performance, we compared the catalysis activities of Co, GO/Co, PEI/Co, and PEI-GO/Co catalysts. All the catalytic reactions were conducted under the same condition (10 mmol L^{-1} catalyst, 90 mmol L^{-1} AB and at 25.0 ± 0.5 °C). Figure 2a presents the time-dependent H_2 evolution volumes of AB hydrolysis catalyzed by the above four catalysts. It is observed that the Co catalyst without any protective agents has a dehydrogenation capability of 2.90 in ~5.5 min (2.90 is the molar ratio of released H_2 to initial AB, that is, H_2/AB = 2.90). When Co was deposited on GO, no discernible increase in the H_2 evolution rate was observed, primarily arising from the aggregation of Co NPs on bare GO sheets. As shown in Supporting Information Figure S6, Co NPs form large clumps or agglomerates due to the lack of ligand protection, which would be the critical cause that resulted in their poor catalytic performance.

The accelerating effect of amine groups on the Co catalyzed AB hydrolysis is surprising and impressive, suggesting a synergistic effect that has never been observed in reported studies. Compared to Co and GO/Co, the catalytic activity of PEI/Co is significantly improved with a total TOF value of 22.8 mol_{H2} min^{-1} mol_{Co}^{-1}, only ~1.2 min needed to release hydrogen of H_2/AB = 2.95. Furthermore, when PEI molecules are decorated on GO surfaces, the resulting PEI-GO/Co catalyst shows an extremely high catalysis activity, with which the hydrolysis is completed to reach H_2/AB = 2.95 only within 0.7 min, showing a total TOF value as high as 39.9 mol_{H2} min^{-1} mol_{Co}^{-1} (the detailed calculation method for total TOF is described in Supporting Information). Compared with other Co-based catalysts (Figure 2b), the PEI-GO/Co catalyst is among the most active Co-based monometallic catalysts, superior to the majority of Co-based multimetallic catalysts and even comparable with the noble metal catalysts, for example, 40% Pt/C and Ru@Al_2O_3.[32,38] We believe that this excellent catalytic activity not only arises from the uniform spatial distribution of small NPs, the morphological control of PEI chains to Co NPs, but also reflects the synergistic effect of amine ligands.

Obviously, the size of NPs is closely related to the number of surface atoms, which usually determines the catalytic activities of metal-based catalysts.[47] As shown in Figure 1c, the distribution of Co NPs on PEI-GO is uniform, with an average diameter of 2.6 nm. Likewise, the FE-SEM image in Supporting Information Figure S5 also shows that tiny NPs uniformly distributed on the PEI-GO surface. These small NPs are highly surface-active, resulting in the improvement in catalytic performance. And then, it is certain that the presence of GO endows Co NPs with more accessible surface active sites. Although the difference in particle size between PEI/Co and PEI-GO/Co is indistinctive (as shown in Figure 1), the PEI-GO/Co exhibits significantly enhanced catalytic activity compared to the former. Without GO, PEI chains prefer to agglomerate into "spheres" when dissolved in aqueous solution.[48] In this case, the encapsulated Co ions in the inner PEI layer become more likely to aggregate after reduction by $NaBH_4$. This makes reduced NPs encapsulated in the interior difficult to contact with AB molecules, and thus displaying a lower catalytic activity for PEI/Co. The presence of GO contributes to prevent the occurrence of the above aggregation phenomenon. Such a thin PEI layer on GO surface is favorable for the diffusion of reducing agent or substrates and correspondingly increases the accessible surface area of Co NPs.

Most of all, the synergistic effect between amine groups and Co NPs is a key factor to achieve high hydrolytic activities of AB. We have controlled the degree of amidation in the PEI-GO composites by adjusting pH of the reaction solution to 11,

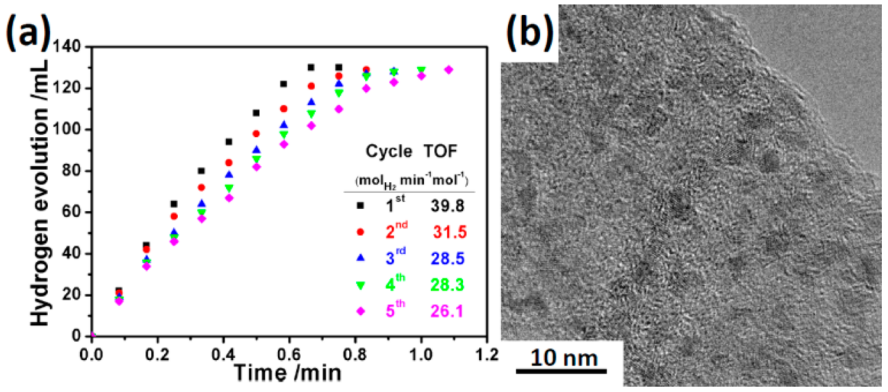

Figure 4. (a) Plot of time vs volume of hydrogen generated from hydrolysis of AB catalyzed by PEI-GO/Co catalysts from 1st to 5th cycle at 25 ± 0.5 °C. (b) HRTEM image after five catalytic cycles.

which contributes to preserve most of amine groups of PEI intact. This also makes the Co NPs deposited on PEI-GO prepared at pH = 11 exhibit much higher catalytic activity than those deposited on PEI-GO prepared under the neutral condition. Given that the same reactants were used for these two samples, the enhanced catalytic performance directly points to the difference in chemical composition or local environment of the resulting samples. We presume that the amine-rich local environment induces a synergistic effect in the course of AB hydrolysis. It has been reported that nitrogen-containing groups would affect the catalytic properties of the embedded metal NPs due to the interaction with the surface metal atoms, resulting in an enhanced hydrogenation rate.[49] At this point, we believe that the amine groups of PEI presumably also offer reactants a unique access pathway to Co NPs and modify their local environment.

To illustrate the unique role that amine ligands play in the dehydrogenation of AB, we designed a series of experiments. We chose some representative capping agents to prepare Co NPs under the identical condition (solution pH value was adjusted to 10 by 0.1 M NaOH and 0.1 M HCl, molar atom ratio [N]/[Co] = 1 for amines and PEI, molar ratio [C(O)N]/[Co] and [COOH]/[Co] = 1 for PVP and poly(acrylic acid) (PAA), including 1,2-ethylenediamine (EDA), triethylamine (TEA), diisopropylamine (DIPA), PVP, PAA, branched PEI (BPEI) and linear PEI (LPEI)). Herein, we unify the molar ratio of functional group of each capping agents to Co atoms for performance comparison. For amine molecules, the molar ratio of [N]/[Co] equals that of amine groups to Co atoms in each system. For polymers, we calculate the moles of amine groups ($n_{\text{amine groups}}$) according to the following method, for example, $n_{\text{amine groups}} = m_{\text{PEI}}/M_{\text{EI}}$, where m_{PEI} and M_{EI} represent the mass of PEI and the molecular weight of ethylene imine (EI) monomer, respectively. Figure 3a shows the initial TOF values (definition is presented in Supporting Information) for bare Co NPs and Co NPs capped with different polymers and amine molecules. As expected, both BPEI- and LPEI-capped Co NPs exhibit equally the best catalytic performance, with initial TOF values of 31.3 and 30.7 mol_{H2} min^{-1} mol_{Co}^{-1}, respectively. By comparison, EDA (a bidentate ligand) as the capping agent of Co NPs reveals a moderate improvement in dehydrogenation efficiency, while for TEA and DIPA (monodentate ligands), only slight improvements are observed. Compared to those polymer amine-based capping agents (BPEI and LPEI), small organic amine molecules (EDA, TEA, and DIPA) have much weaker capability in morphological control during the formation of Co NPs, which makes the resulting NPs have larger particle sizes and even aggregates, see Supporting Information Figure S7. Nevertheless, these amine molecule-capped Co NPs still exhibit obviously superior dehydrogenation efficiency to Co NPs capped with PAA and PVP. These experimental facts apparently reflect the key role of amine-rich polymers (BPEI and LPEI) in controlling morphology of NPs and amine groups in prompting the hydrolysis of AB.

Moreover, it has been recognized that even after the reduction of metal ions, ligand molecules still have ability to form weak coordination with metal particles through multiple sites.[50,51] This implies that polydentate amine ligands such as BPEI and LPEI have larger possibility, relative to bidentate and monodentate ligands, to chelate with Co^{2+} ions and then to confine the reduced Co NPs within polymer frameworks through coordination and steric separation. Similar studies have been reported by Mao et al., where BWT, as a polyphenol provided excellent chelating ability with Ru^{3+} and Pd^{2+} to form size-controlled and highly stable metal complexes catalyst. By comparison, monodentate ligand-chelated metal catalysts only showed poor stability during the reaction.[52]

The synergistic effect of amine ligands may also be further confirmed by examining the effect of PAA and PVP on the catalytic activity of Co NPs, which allows us to exclude the interference of particle size. PAA and PVP are two capping agents that commonly used to control the morphology of NPs.[43,53]As shown in Figure 3a, however, both PAA/Co and PVP/Co show poor catalytic activity to the dehydrogenation of AB, although the particle sizes of Co NPs in these two systems are far smaller than that of EDA/Co NPs, see Supporting Information Figure S7. This strongly suggests that amine-based capping agents are important for prompting the Co catalyzed dehydrogenation.

As mentioned previously, the synergistic effect of amine–capped Co NPs is also related to the local environment of metal particles. To illustrate the significant influence of the local environment, we changed the amounts of amine groups and varied the molar ratio of [N]/[Co] in PEI/Co. The initial TOF values of AB dehydrogenation for these PEI/Co catalysts are shown in Figure 3b. Clearly, the PEI/Co catalyst with the molar ratio [N]/[Co] = 1 exhibited the highest dehydrogenation rate, and then the dehydrogenation rate decreased with increasing PEI contents. This strong dependence on the ligand concentration indicates the influence of the extent of exposed metal particle surface to the reactant (AB). A higher

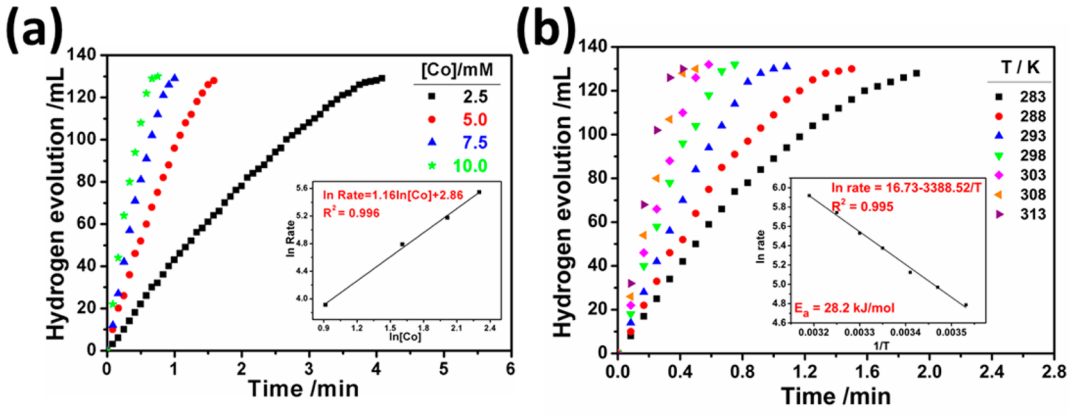

Figure 5. Kinetics study of PEI-GO/Co catalysts: (a) hydrolysis of AB at different concentrations of PEI-GO/Co NPs (inset, plot of ln rate vs ln[Co]) and (b) hydrolysis of AB at different temperatures (inset, Arrhenius plot of ln rate vs $1/T$).

concentration of capping ligand implies a larger surface coverage to metal particle surface, which either blocks accessible active sites, or inhibits the occurrence of catalytic reactions due to limited active metal surfaces.[54] To further verify such an effect, we conducted UV−vis observation for PEI-Co^{2+} samples with different molar ratios. As shown in Supporting Information Figure S1, the intensity of the characteristic peak at 224 nm increases with increasing amounts of PEI and reaches the saturation value at a [N]/[Co] ratio of 9. Therefore, Co^{2+} ions tend to chelate with more amine ligands at higher [N]/[Co] molar ratios before the saturation, leading to greater steric crowding and decreased accessible surface area of Co NPs surface. As a result, both the local environment of the active sites and the reaction pathway (adsorption/desorption for AB) may be changed in this case. Apparently, it is likewise important to optimize the amount of ligand on metal surface and the local environment of active sites for improving the catalytic performance of amine-capped metal NPs.

3.3. Reusability of PEI-GO/Co Catalyst. As an AB dehydrogenation catalyst, excellent stability and reusability are desired. The synthesized PEI-GO/Co NPs are somewhat magnetic and thus may be separated readily by an external magnet (Supporting Information Figure S9), providing a convenient recycling approach. Figure 4a shows the catalytic ability of PEI-GO/Co after recycling 5 times. It is observed that the time to complete AB dehydrogenation gradually increases with increasing cycles, implying the decreased catalytic activity. After experiencing the fifth cycle, the catalyst retains 65.6% of its initial catalytic activity. TEM images (Figures 1c and 4b) indicate that there are no obvious change in size and morphology of Co NPs after five cycles. Also, XRD results (Supporting Information Figure S4) prove that no reaction-reduced crystalline phase appeared during the cycling test. On the basis of these facts, it is presumed that several factors probably affect the reusability of the PEI-GO/Co catalysts. The first one is that the hydrolysis of AB could engender the formation of byproducts such as BO_2^-, which passivates the surface of NPs.[55,56] Besides, in our recycling experiments, all tests were conducted in air. Small Co NPs are practically highly sensitive to oxygen in air due to their abundant surface atoms, which is confirmed by the XPS results in Supporting Information Figure S10. We find that a considerable proportion of Co atoms are in the oxidation state of the fresh prepared PEI-GO/Co catalyst. As is verified in most papers, the inactivation of surface atoms of NPs due to the oxidation in air should be accounted for the degradation of performance during the reusable process.[33,46] Thus, oxidation of Co NPs cannot be ignored for the decreased reusable performance here. Meanwhile, the possible leaching of Co NP into solution may damage the performance at a certain degree.[57] Nevertheless, the high catalytic activity of PEI-GO/Co for the hydrolysis of AB still provides a promising approach for future applications in hydrogen energy economy.

3.4. Kinetics Study of PEI-GO/Co Catalysts. The kinetics of PEI-GO/Co-catalyzed AB hydrolysis were studied under different catalyst concentrations and reaction temperatures. The kinetics of AB hydrolysis provides valuable information on what factors control the dehydrogenation rate and possible mechanism routes.

The effect of the amount of PEI-GO/Co on the dehydrogenation rate was investigated by the hydrolysis of 90 mM AB solution at 25 °C with varying PEI-GO/Co amounts (2.5, 5.0, 7.5, and 10 mM) while keeping other parameters constant. The results are presented in Figure 5a. The reaction rates (mL min^{-1}) at different catalyst contents are calculated from the slope of the linear part of each curve. With increasing content of the catalyst from 2.5 to 10.0 mM, the average H_2 evolution rate increases remarkably under the condition of releasing equivalent H_2. Hence, the rate of H_2 generation can be controlled by adjusting the concentration of the catalyst. Figure 5a shows the change of reaction time with volume of released H_2 at different Co contents. The plot of H_2 evolution rate versus Co content in logarithmic scale, with a slope of 1.16, in the inset of Figure 5a indicates the first-order kinetics with respect to the catalyst concentration for the Co-catalyzed AB hydrolysis.

Figure 5b shows the plot of reaction time versus volume of H_2 generated at different temperatures. It is clear that the H_2 evolution rate increases gradually with increasing solution temperatures from 10 to 40 °C, indicating that a high reaction temperature is beneficial for enhancing the hydrogenation rate. According to the Arrhenius plot of ln (r) versus 1/T, in the inset of Figure 5b, the obtained slope (i.e., activation energy) is 28.2 kJ mol^{-1}. This is relatively a low value, as compared to those reported single cobalt-based catalysts (Figure 2b). In other words, there probably exists preferred pathways for AB molecules to form activated species on NPs surface, which drives us to further explore the possible mechanism.

Scheme 1. Proposed Mechanism for PEI-GO/Co Catalyzed Dehydrogenation Hydrolysis of NH_3BH_3: (1) Diffusion of AB; (2) Dihydrogen Bond Formation; (3) Activation and Attack Process; (4) Hydrolysis of AB

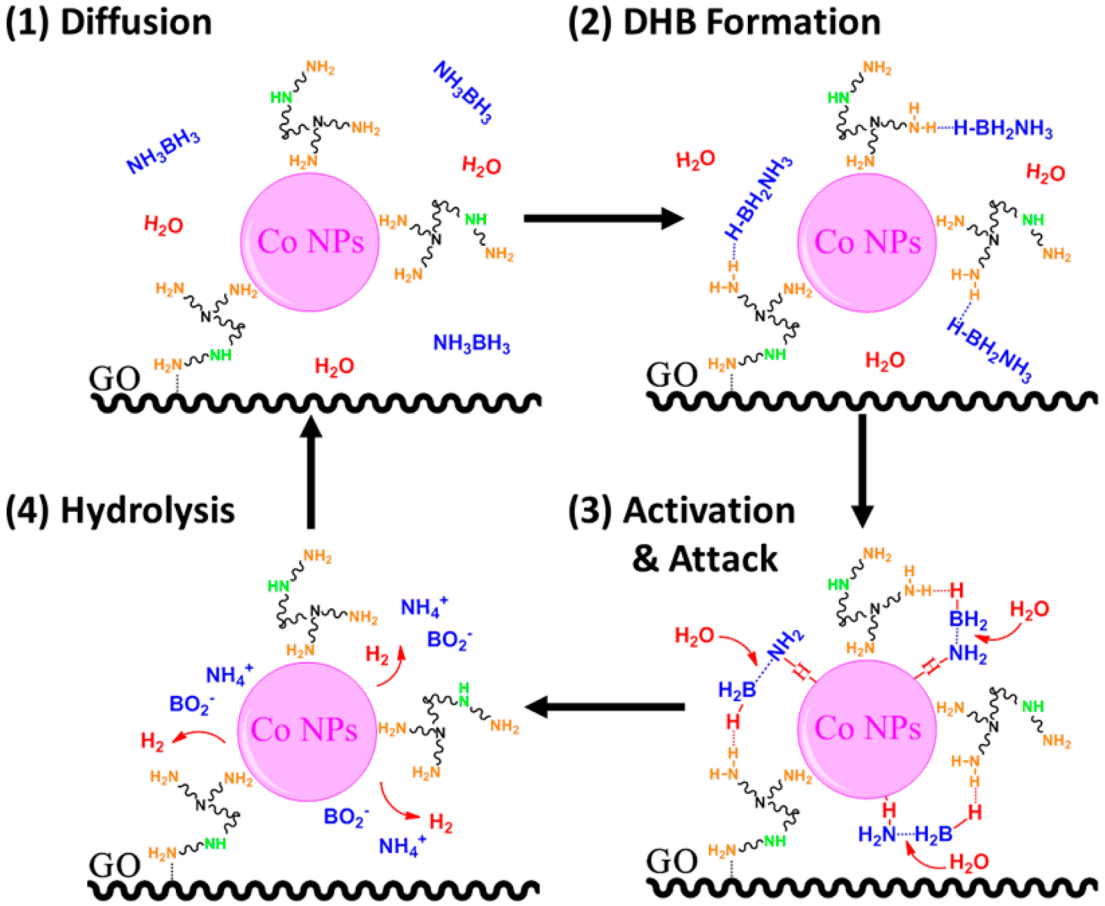

3.5. Assumption of Amine-Prompted Dehydrogenation Mechanism. Xu et al. have suggested that the dehydrogenation mechanism of AB in the presence of non-noble metal catalysts (e.g., Co NPs) might involve three steps: (1) formation of activated complex species on metal particle surface; (2) concerted dissociation of the B−N bonding because of the attack of H_2O molecules; and (3) hydrolysis of the resulting BH_3 intermediate to produce H_2.[42] In addition, $NaBH_4$ (SB) may be used as a hydrogen storage material or as a fuel of direct fuel cell with a reaction activity higher than that of AB. For SB, it does not need a dissociation process to release H_2 and it could self-hydrolyze in water.[58] This implies that SB should have an equal or even higher H_2 generation rate than AB in aqueous/basic solutions. As demonstrated by Özkar et al.,[43] when PVP-stabilized Cobalt(0) nanoclusters were used to catalyze SB hydrolysis at 298 K, it revealed a rate constant (0.034) similar to that of AB (0.033) in neutral aqueous solution. Indeed, the highest H_2 evolution rate of SB in aqueous solution has been found to be 560 L_{H2} min^{-1} $g_{catalyst/metal}^{-1}$, far higher than 122 L_{H2} min^{-1} $g_{catalyst/metal}^{-1}$ of AB.[58] However, this seems to be different from our experimental observation in the PEI-GO/Co catalyzed AB dehydrogenation. The Co NP catalyzed hydrolysis reveals nearly identical H_2 evolution rates for SB and AB; however, the PEI-GO/Co catalyzed AB hydrolysis exhibits a H_2 evolution rate much faster (>4 times, see Supporting Information Figure S11) than that of SB under the same condition. This unique phenomenon indicates PEI is not silent in the hydrolysis of AB. It is not only a simple stabilizer, but also provides a more superior reactive pathway for AB to dehydrogenation on the metal surface with the assistance of amine groups. Recalling the accelerating effect of amine ligands observed in Figure 3a, along with the low calculated activation energy (28.2 kJ mol^{-1}) for PEI-GO/Co catalysts and the difference between PEI-GO/Co catalyzed hydrolysis of AB and SB, we present our fundamental understandings on this amine-prompted dehydrogenation mechanism hereinafter.

As mentioned above, the primary difference between AB and SB lies in the B−N bond in AB molecules. We propose that the contribution of the amine ligands may come from the following routes: (1) amine ligand combines with Co surface to produce protonic hydrogens, which would interact with the hydridic hydrogens of "BH_3" part of AB to form dihydrogen bonds (DHBs); (2) the dihydrogen complexes help to reduce the energy barrier of AB molecules to form activated species with Co NPs afterward. As pointed out by Chen et al., DHBs have a strength comparable to conventional hydrogen bonds and are common in AB chemistry.[59] Furthermore, DHBs play a dominant role in dictating the reaction pathways where oppositely charged hydrogens coexist for DHB formation.[59] Similarly, Nguyen et al. proposed that Ru-complex bearing cooperative PNP ligands could form dihydrogen complex with AB to promote the exchange and elimination of hydrogen, effectively reducing the energy barrier for H_2 release.[60]

Therefore, we propose a mechanism to explain the ultrahigh activity of PEI-GO/Co catalysts observed in AB dehydrogen-

ation, whose primary route is presented in Scheme 1. The first step of the reaction is a diffusion process of AB. Because of the formation of DHBs between AB and amine groups of PEI, AB molecules are concentrated near the surface of PEI-GO/Co catalysts, leading to a higher local AB concentration than that the bulk solution. Subsequently, these AB molecules near the NP surface are activated due to the interaction of "N−H" bonds with the metal center. Meanwhile, owing to the DHBs forming with amine groups of PEI, some AB molecules are converted into the activated species containing "−NH···HBH_2−" bonds. This effectively reduces the activation barrier and weakens the "B−N" bonds of AB molecules. We believe that such an activation process that involves the DHBs induced local AB concentration near the catalyst surface is critical for the observed high H_2 evolution rate. Finally, the hydrolysis of AB is completed by the attack of H_2O molecules to these weakened "B−N" bonds, followed by the hydrolysis of the BH_3 intermediate to release H_2.What should be mentioned is that although we have tentatively proposed a dehydrogenation mechanism to rationalize our experimental observation on the basis of our and other groups' studies, further systematic studies are still necessary, which are in pursuing in our group and will be discussed in separate reports. In view of the prominent catalytic activity of amine-capped transition metal NPs and their unique catalytic mechanism, we expect this novel amine-prompted dehydrogenation concept facilitates to open a valuable pathway for developing high performance heterogeneous catalysts.

4. CONCLUSIONS

The present work demonstrates the validity of amine-rich polymers such as branched or linear PEI to control the morphology, spatial and size distributions, formation of activated intermediate species and local environment near the metal surface. The amine groups of PEI are able to chelate with metal ions such as Co^{2+}, resulting in small-sized, amorphous Co NPs on PEI-GO support with uniform spatial and size distributions, as well as partial coverage of Co surfaces. Since amine-rich PEI molecules are highly affine to AB, the DHBs formation between amine groups and -BH_3 part of AB generates a local environment with a high AB concentration near Co NPs, which also prompts the formation of activated intermediate species and lowers the energy barrier for the dehydrogenation of AB, resulting in a dramatically enhanced hydrogen evolution rate. Our results indicate the importance of amine ligands for optimizing the dehydrogenation efficiency of AB. With the use of such capping agents, PEI-GO/Co catalysts exhibit high dehydrogenation efficiency, a total turnover frequency as high as 39.9 mol_{H_2} min^{-1} $mol_{Co}{}^{-1}$ and a low apparent activation energy of 28.2 kJ mol^{-1}. This makes them one of the best Co-based dehydrogenation catalyst, and even comparable to the catalytic performance of noble metal-containing multimetal catalysts. In the proposed tentative mechanism, we believe that the concentration of AB near the NPs surface, activated intermediate species and local environment favorable to their formation are critical for improving the dehydrogenation of AB. We expect that this new finding can facilitate the development practically applicable energy storage materials.

■ ASSOCIATED CONTENT

Supporting Information

TGA curves, FT-IR, XPS, UV−vis spectra of PEI-GO composites; FE-SEM, TEM images of the PEI-GO/Co catalysts; microscopy evidence of the deposition of Co NPs on various materials; TEM images of the crystallization of the NPs; H_2 generation rates of AB and SB using PEI-GO/Co catalysts and definition of the initial TOF, etc. This material is available free of charge via the Internet at http://pubs.acs.org.

■ AUTHOR INFORMATION

Corresponding Author

*E-mail: hongbinlu@fudan.edu.cn. Tel/Fax: +86-21-55664589.

Funding

This work was supported by National Basic Research Program of China (grant no. 2011CB605702), NSF of China (grant no. 50573014, 50773012 and 51173027), Shanghai Nanotechnology Program (grant no. 1052 nm00400), and Shanghai Basic Research Program (grant no. 14JC1400600).

Notes

The authors declare no competing financial interest.

■ ACKNOWLEDGMENTS

We thank Ms. Limin Sun (Shanghai Jiao Tong University) for her assistance with XPS. We also appreciate Prof. Renchao Che, Prof. Ping Zhou, and Prof. Minghua Qiao (Fudan University) for their valuable comments.

■ REFERENCES

(1) Young, S. Global Energy Prospects. *Nature* **2001**, *414*, 487−488.
(2) Dresselhaus, M. S.; Thomas, I. L. Alternative Energy Technologies. *Nature* **2001**, *414*, 332−337.
(3) Schlapbach, L.; Züttel, A. Hydrogen-Storage Materials for Mobile Applications. *Nature* **2001**, *414*, 353−358.
(4) Peng, B.; Chen, J. Ammonia Borane as an Efficient and Lightweight Hydrogen Storage Medium. *Energy Environ. Sci.* **2008**, *1*, 479−483.
(5) Tang, Z.; Chen, X.; Chen, H.; Wu, L.; Yu, X. Metal-Free Catalysis of Ammonia-Borane Dehydrogenation/Regeneration for a Highly Efficient and Facilely Recyclable Hydrogen-Storage Material. *Angew. Chem., Int. Ed.* **2013**, *52*, 5832−5835.
(6) Huang, Z.; Autrey, T. Boron−Nitrogen−Hydrogen (BNH) Compounds: Recent Developments in Hydrogen Storage, Applications in Hydrogenation and Catalysis, and New Syntheses. *Energy Environ. Sci.* **2012**, *5*, 9257−9268.
(7) Metin, Ö.; Mazumder, V.; Özkar, S.; Sun, S. Monodisperse Nickel Nanoparticles and Their Catalysis in Hydrolytic Dehydrogenation of Ammonia Borane. *J. Am. Chem. Soc.* **2010**, *132*, 1468−1469.
(8) Rakap, M.; Özkar, S. Hydroxyapatite-Supported Cobalt(0) Nanoclusters as Efficient and Cost-Effective Catalyst for Hydrogen Generation from the Hydrolysis of Both Sodium Borohydride and Ammonia-Borane. *Catal. Today* **2012**, *183*, 17−25.
(9) Zhang, L.; Tu, Q.; Chen, X.; Liu, P. Nano Metal Catalysts in Dehydrogenation of Ammonia Borane. *Prog. Chem.* **2014**, *5*, 749−755.
(10) Qiu, F.; Li, L.; Liu, G.; Wang, Y.; An, C.; Xu, C.; Xu, Y.; Wang, Y.; Jiao, L.; Yuan, H. Synthesis of $Fe_{0.3}Co_{0.7}$/rGO Nanoparticles as a High Performance Catalyst for the Hydrolytic Dehydrogenation of Ammonia Borane. *Int. J. Hydrogen Energy* **2013**, *38*, 7291−7297.
(11) Metin, Ö.; Dinç, M.; Eren, Z. S.; Özkar, S. Silica Embedded Cobalt(0) Nanoclusters: Efficient, Stable and Cost Effective Catalyst for Hydrogen Generation from the Hydrolysis of Ammonia Borane. *Int. J. Hydrogen Energy* **2011**, *36*, 11528−11535.
(12) Yen, H.; Kleitz, F. High-Performance Solid Catalysts for H_2 Generation from Ammonia Borane: Progress through Synergetic Cu−Ni Interactions. *J. Mater. Chem. A* **2013**, *1*, 14790−14796.

(13) Zhu, Q. L.; Li, J.; Xu, Q. Immobilizing Metal Nanoparticles to Metal−Organic Frameworks with Size and Location Control for Optimizing Catalytic Performance. *J. Am. Chem. Soc.* **2013**, *135*, 10210−10213.
(14) Xi, P.; Chen, F.; Xie, G.; Ma, C.; Liu, H.; Shao, C.; Wang, J.; Xu, Z.; Xu, X.; Zeng, Z. Surfactant Free RGO/Pd Nanocomposites as Highly Active Heterogeneous Catalysts for the Hydrolytic Dehydrogenation of Ammonia Borane for Chemical Hydrogen Storage. *Nanoscale* **2012**, *4*, 5597−5601.
(15) Çalışkan, S.; Zahmakıran, M.; Özkar, S. Zeolite Confined Rhodium(0) Nanoclusters as Highly Active, Reusable, and Long-Lived Catalyst in the Methanolysis of Ammonia-Borane. *Appl. Catal., B* **2010**, *93*, 387−394.
(16) Akbayrak, S.; Özkar, S. Ruthenium(0) Nanoparticles Supported on Multiwalled Carbon Nanotube as Highly Active Catalyst for Hydrogen Generation from Ammonia-Borane. *ACS Appl. Mater. Interfaces* **2012**, *4*, 6302−6310.
(17) Karahan, S.; Zahmakiran, M.; Özkar, S. A Facile One-Step Synthesis of Polymer Supported Rhodium Nanoparticles in Organic Medium and Their Catalytic Performance in the Dehydrogenation of Ammonia-Borane. *Chem. Commun.* **2012**, *48*, 1180−1182.
(18) Zahmakiran, M.; Özkar, S. Transition Metel Nanoparticles in Catalysis for the Hydrogen Generation from the Hydrolysis of Ammonia-Borane. *Top. Catal.* **2013**, *56*, 1171−1183.
(19) Niu, Z.; Li, Y. Removal and Utilization of Capping Agents in Nanocatalysis. *Chem. Mater.* **2014**, *26*, 72−83.
(20) Wu, B.; Zheng, N. Surface and Interface Control of Noble Metal Nanocrystals for Catalytic and Electrocatalytic Applications. *Nano Today* **2013**, *8*, 168−197.
(21) Yang, L.; Luo, W.; Cheng, G. Graphene-Supported Ag-Based Core−Shell Nanoparticles for Hydrogen Generation in Hydrolysis of Ammonia Borane and Methylamine Borane. *ACS Appl. Mater. Interfaces* **2013**, *5*, 8231−8240.
(22) Zhang, Q.; Lee, I.; Joo, J. B.; Zaera, F.; Yin, Y. Core−Shell Nanostructured Catalysts. *Acc. Chem. Res.* **2013**, *46*, 1816−1824.
(23) Feng, W.; Yang, L.; Cao, N.; Du, C.; Dai, H.; Luo, W.; Cheng, G. In Situ Facile Synthesis of Bimetallic CoNi Catalyst Supported on Graphene for Hydrolytic Dehydrogenation of Amine Borane. *Int. J. Hydrogen Energy* **2014**, *39*, 3371−3380.
(24) Qiu, F.; Liu, G.; Li, L.; Wang, Y.; Xu, C.; An, C.; Chen, C.; Xu, Y.; Huang, Y.; Wang, Y.; Jiao, l.; Yuan, H. Synthesis of Triple-Layered Ag@Co@Ni Core−Shell Nanoparticles for the Catalytic Dehydrogenation of Ammonia Borane. *Chem.—Eur. J.* **2014**, *20*, 505−509.
(25) Qiu, F.; Li, L.; Liu, G.; Xu, C.; An, C.; Xu, Y.; Wang, Y.; Huang, Y.; Chen, C.; Wang, Y. Synthesis of Size-Controlled Ag@Co@Ni/Graphene Core−Shell Nanoparticles for the Catalytic Hydrolysis of Ammonia Borane. *Chem.—Asian J.* **2014**, *9*, 487−493.
(26) Taguchi, T.; Isozaki, K.; Miki, K. Enhanced Catalytic Activity of Self-Assembled-Monolayer-Capped Gold Nanoparticles. *Adv. Mater.* **2012**, *24*, 6462−6467.
(27) Wu, B.; Huang, H.; Yang, J.; Zheng, N.; Fu, G. Selective Hydrogenation of α,β-Unsaturated Aldehydes Catalyzed by Amine-Capped Platinum−Cobalt Nanocrystals. *Angew. Chem., Int. Ed.* **2012**, *51*, 3440−3443.
(28) Stowell, C. A.; Korgel, B. A. Iridium Nanocrystal Synthesis and Surface Coating-Dependent Catalytic Activity. *Nano Lett.* **2005**, *5*, 1203−1207.
(29) Chen, S.; Wei, Z.; Qi, X.; Dong, L.; Guo, Y. G.; Wan, L.; Shao, Z.; Li, L. Nanostructured Polyaniline-Decorated Pt/C@PANI Core−Shell Catalyst with Enhanced Durability and Activity. *J. Am. Chem. Soc.* **2012**, *134*, 13252−13255.
(30) Tsunoyama, H.; Ichikuni, N.; Sakurai, H.; Tsukuda, T. Effect of Electronic Structures of Au Clusters Stabilized by Poly(*N*-Vinyl-2-pyrrolidone) on Aerobic Oxidation Catalysis. *J. Am. Chem. Soc.* **2009**, *131*, 7086−7093.
(31) Wang, X.; Yang, J.; Yin, H.; Song, R.; Tang, Z. "Raisin Bun"-Like Nanocomposites of Palladium Clusters and Porphyrin for Superior Formic Acid Oxidation. *Adv. Mater.* **2013**, *25*, 2728−2732.
(32) Xu, Q.; Chandra, M. A Portable Hydrogen Generation System: Catalytic Hydrolysis of Ammonia−Borane. *J. Alloys Compd.* **2007**, *446−447*, 729−732.
(33) Zhou, X.; Chen, Z.; Yan, D.; Lu, H. Deposition of Fe−Ni Nanoparticles on Polyethyleneimine-Decorated Graphene Oxide and Application in Catalytic Dehydrogenation of Ammonia Borane. *J. Mater. Chem.* **2012**, *22*, 13506−13516.
(34) Yu, D.; Dai, L. Self-Assembled Graphene/Carbon Nanotube Hybrid Films for Supercapacitors. *J. Phys. Chem. Lett.* **2010**, *1*, 467−470.
(35) Zhang, Y.; Chen, B.; Zhang, L.; Huang, J.; Chen, F.; Yang, Z.; Yao, J.; Zhang, Z. Controlled Assembly of Fe_3O_4 Magnetic Nanoparticles on Graphene Oxide. *Nanoscale* **2011**, *3*, 1446−1450.
(36) Sui, Z.; Cui, Y.; Zhu, J.; Han, B. Preparation of Three-Dimension Graphene Oxide-Polyethylenimine Porous Materials as Dye and Gas Adsorbents. *ACS Appl. Mater. Interfaces* **2013**, *5*, 9172−9179.
(37) Kobayashi, S.; Suh, K. D.; Shirokura, Y. Chelating Ability of Poly(Vinylamine): Effects of Polyamine Structure on Chelation. *Macromolecules* **1989**, *22*, 2363−2366.
(38) Can, H.; Metin, Ö. A Facile Synthesis of Nearly Monodisperse Ruthenium Nanoparticles and Their Catalysis in the Hydrolytic Dehydrogenation of Ammonia Borane for Chemical Hydrogen Storage. *Appl. Catal., B* **2012**, *125*, 304−310.
(39) Yan, J.-M.; Zhang, X.-B.; Shioyama, H.; Xu, Q. Room Temperature Hydrolytic Dehydrogenation of Ammonia Borane Catalyzed by Co Nanoparticles. *J. Power Sources* **2010**, *195*, 1091−1094.
(40) Metin, Ö.; Özkar, S. Water Soluble Nickel(0) and Cobalt(0) Nanoclusters Stabilized by Poly(4-Styrenesulfonic Acid-co-maleic Acid): Highly Active, Durable and Cost Effective Catalysts in Hydrogen Generation from the Hydrolysis of Ammonia Borane. *Int. J. Hydrogen Energy* **2011**, *36*, 1424−1432.
(41) Figen, A. K. Dehydrogenation Characteristics of Ammonia Borane via Boron-Based Catalysts (Co−B, Ni−B, Cu−B) under Different Hydrolysis Conditions. *Int. J. Hydrogen Energy* **2013**, *38*, 9186−9197.
(42) Xu, Q.; Chandra, M. Catalytic Activities of Non-Noble Metals for Hydrogen Generation from Aqueous Ammonia−Borane at Room Temperature. *J. Power Sources* **2006**, *163*, 364−370.
(43) Metin, Ö.; Özkar, S. Hydrogen Generation from the Hydrolysis of Ammonia-Borane and Sodium Borohydride Using Water-Soluble Polymer-Stabilized Cobalt(0) Nanoclusters Catalyst. *Energy Fuels* **2009**, *23*, 3517−3526.
(44) Rachiero, G. P.; Demirci, U. B.; Miele, P. Bimetallic RuCo and RuCu Catalysts Supported on γ-Al_2O_3. A Comparative Study of Their Activity in Hydrolysis of Ammonia-Borane. *Int. J. Hydrogen Energy* **2011**, *36*, 7051−7065.
(45) Sun, D.; Mazumder, V.; Metin, Ö.; Sun, S. Catalytic Hydrolysis of Ammonia Borane via Cobalt Palladium Nanoparticles. *ACS Nano* **2011**, *5*, 6458−6464.
(46) Yang, L.; Su, J.; Meng, X.; Luo, W.; Cheng, G. In Situ Synthesis of Graphene Supported Ag@CoNi Core−Shell Nanoparticles as Highly Efficient Catalysts for Hydrogen Generation from Hydrolysis of Ammonia Borane and Methylamine Borane. *J. Mater. Chem. A* **2013**, *1*, 10016−10023.
(47) Wang, C.; van der Vliet, D.; Chang, K.-C.; You, H.; Strmcnik, D.; Schlueter, J. A.; Markovic, N. M.; Stamenkovic, V. R. Monodisperse Pt_3Co Nanoparticles as a Catalyst for the Oxygen Reduction Reaction: Size-Dependent Activity. *J. Phys. Chem. C* **2009**, *113*, 19365−19368.
(48) Schneider, M.; Brinkmann, M.; Möhwald, H. Adsorption of Polyethylenimine on Graphite: An Atomic Force Microscopy Study. *Macromolecules* **2003**, *36*, 9510−9518.
(49) Králik, M.; Biffis, A. A. Catalysis by Metal Nanoparticles Supported on Functional Organic Polymers. *J. Mol. Catal. A: Chem.* **2001**, *177*, 113−138.

(50) Teranishi, T.; Miyake, M. Size Control of Palladium Nanoparticles and Their Crystal Structures. *Chem. Mater.* **1998**, *10*, 594−600.
(51) Zhang, Y.; Grass, M. E.; Kuhn, J. N.; Tao, F.; Habas, S. E.; Huang, W.; Yang, P.; Somorjai, G. A. A. Highly Selective Synthesis of Catalytically Active Monodisperse Rhodium Nanocubes. *J. Am. Chem. Soc.* **2008**, *130*, 5868−5869.
(52) Mao, H.; Yu, H.; Chen, J.; Liao, X. Biphasic Catalysis Using Amphiphilic Polyphenols-Chelated Noble Metals as Highly Active and Selective Catalysts. *Sci. Rep.* **2013**, *3*, 2226.
(53) Chen, Z.-C.; Ring, T. A.; Lemaitre, J. Stabilization and Processing of Aqueous $BaTiO_3$ Suspension with Polyacrylic Acid. *J. Am. Ceram. Soc.* **1992**, *75*, 3201−3208.
(54) Watzky, M. A.; Finke, R. G. Transition Metal Nanocluster Formation Kinetic and Mechanistic Studies. A New Mechanism When Hydrogen Is the Reductant: Slow, Continuous Nucleation and Fast Autocatalytic Surface Growth. *J. Am. Chem. Soc.* **1997**, *119*, 10382−10400.
(55) Clark, T. J.; Whittell, G. R.; Manners, I. Highly Efficient Colloidal Cobalt- and Rhodium-Catalyzed Hydrolysis of $H_3N{\cdot}BH_3$ in Air. *Inorg. Chem.* **2007**, *46*, 7522−7527.
(56) Jaska, C. A.; Clark, T. J.; Clendenning, S. B.; Grozea, D.; Turak, A.; Lu, Z. H.; Manners, I. Poisoning of Heterogeneous, Late Transition Metal Dehydrocoupling Catalysts by Boranes and Other Group 13 Hydrides. *J. Am. Chem. Soc.* **2005**, *127*, 5116−5124.
(57) Patel, N.; Miotello, A.; Bello, V. Pulsed Laser Deposition of Co-Nanoparticles Embedded on B-Thin Film: A Very Efficient Catalyst Produced in a Single-Step Process. *Appl. Catal., B* **2011**, *103*, 31−38.
(58) Demirci, U. B.; Miele, P. Sodium Borohydride Versus Ammonia Borane, in Hydrogen Storage and Direct Fuel Cell Applications. *Energy Environ. Sci.* **2009**, *2*, 627−637.
(59) Chen, X.; Zhao, J.; Shore, S. The Roles of Dihydrogen Bonds in Amine Borane Chemistry. *Acc. Chem. Res.* **2013**, *46*, 2666−2675.
(60) Swinnen, S.; Nguyen, V. S.; Nguyen, M. T. Hydrogen Release from Ammonia Borane and Derivatives in the Presence of a Ruthenium Complex Incorporating Cooperative PNP Ligands. *Chem. Phys. Lett.* **2011**, *513*, 195−200.